IEEE Access
Multidisciplinary | Rapid Review | Open Access Journal

Received August 1, 2018, accepted September 2, 2018, date of publication September 6, 2018,
date of current version September 28, 2018.

Digital Object Identifier 10.1109/ACCESS.2018.2868989

Compact Broadband Omnidirectional Radiation Pattern Printed Dipole Antenna Incorporated With Split-Ring Resonators

KAM EUCHARIST KEDZE, HEESU WANG, AND IKMO PARK
Department of Electrical and Computer Engineering, Ajou University, Suwon 16499, South Korea

Corresponding author: Ikmo Park (ipark@ajou.ac.kr)

This work was supported in part by the Institute for Information & Communications Technology Promotion (IITP) Grant through the Korean Government (MSIP), University ICT Basic Research Lab, under Grant 2017-0-00959, in part by the Human Resources Program in Energy Technology of the Korea Institute of Energy Technology Evaluation and Planning (KETEP), the Ministry of Trade, Industry & Energy, South Korea, under Grant 20164030201380.

ABSTRACT A broadband, low-profile, compact, and cost-effective antenna consisting of a printed dipole loaded with split-ring resonators (SRRs) is presented. The antenna consists of two identical printed SRRs, each enclosing an arm of a printed dipole element. Each SRR and the center-fed half-wavelength dipole element are printed on the top and bottom sides of a thin dielectric substrate. The dipole is excited by a coaxial feed, while the SRRs are electromagnetically coupled to the dipole. The dipole, in conjunction with the SRRs, generates three resonant modes with stable omnidirectional radiation patterns. These resonances interact to provide broadband characteristics, that is, a measured impedance bandwidth covering 1.32–2.46 GHz for a reflection coefficient of less than −10 dB. The functionalities, mechanisms, and modes of operation of the composite antenna structure are discussed in relation to both the dipole and the SRRs. A prototype is fabricated and measured in order to validate the antenna design. It is computationally and experimentally confirmed that the antenna demonstrates broadband characteristics as well as a stable gain with non-deteriorating omnidirectional radiation patterns. The compact antenna, which has the overall dimensions of 9.6 mm × 74.4 mm × 0.508 mm ($0.06\lambda \times 0.469\lambda \times 0.0032\lambda$ at 1.895 GHz), has a measured fractional bandwidth of 60.31%, an omnidirectional radiation pattern with a gain greater than 1.8 dBi, and a radiation efficiency greater than 88% within a broad impedance bandwidth. The compact size, simple structure, and stable radiation properties of the antenna render it suitable for many wireless communication applications.

INDEX TERMS Broadband antennas, compact, composite antennas, dipole antennas, omnidirectional radiation pattern, split-ring resonator (SRR).

I. INTRODUCTION

The rapid development of wireless communication systems and the associated applications in recent years has necessitated the design of antennas that are able to meet the persistent requirements of current wireless communication applications. The antennas used for such applications are characterized by a wide operating bandwidth, compact size, low cost, and low profile. It is feasible to meet each of these antenna requirements independently; however, merging them within a single antenna design remains a great challenge [1]. Hence, antenna designers and engineers have developed different techniques to meet these antenna requirements [2]–[6]. The use of printed antennas is a practicable approach due to their simple structure and miniature size allowing for easy integration into small devices. In the case of some printed antenna designs, such as dipole antennas and coplanar waveguide-fed monopole antennas [7]–[9], broadband characteristics are generated using composite structures of dipoles and monopole-like radiators. However, some of these antennas are too large in geometric terms, which renders them unsuitable for use in small devices, particularly at very low frequencies. In an attempt to develop wideband antennas, the concept of multi-resonance has been utilized and multi-resonant microstrip patch antennas have been designed [10]–[11]. However, [10] and [11] provide more complexity in geometry but less impedance bandwidth due to the nature of microstrip structure. Another category of antenna design that is widely used in wireless systems is

the loop antenna. Several loops and loop-dipoles have been reported to achieve wideband characteristics [1], [12]–[14]. A small broadband antenna composed of a dual-meander folded loop and a disk-loaded monopole has been designed, although it was found to feature limited and thus inapplicable bandwidth for current broadband systems [14]. The dual-band composite loop-dipole used in [15] exhibited a large bandwidth, but it also involved complicated geometry, including a two-layer substrate, which increased the difficulty of fabrication and reduced the cost effectiveness. The design of a wideband antenna with stable omnidirectional radiation patterns using the theory of characteristic modes is presented in [16]. The antenna is composed of a dipole and single loop to generate two resonant modes with stable radiation patterns.

In order to meet the design requirements, low-profile and compact split-ring resonators (SRRs) have been widely used to develop electrically small antennas (ESAs). The potential for the miniaturization of SRRs, as well as their ability to produce strong electromagnetic resonance, yields a viable technique with which antenna designers and engineers can overcome the problems detailed above [17]. SRRs have been designed to realize dual-band operation and provide a low-profile, compact structure [18]–[20]. However, the reduction in the electrical size results in an increase in the Q-factor, which in turn leads to an undesired reduction in bandwidth [17]. In addition, although the antennas described above exhibit good performance characteristics, they remain inadequate in terms of either the bandwidth, profile, cost, or compactness.

A challenging issue faced by antenna designers and engineers in the design of composite antennas loaded with SRRs concerns the production of stable and non-deteriorating radiation patterns, particularly at high frequencies [17]–[23]. In [17], a triple-band ESA was constructed by integrating three concentric and co-directional SRRs with different dimensions. The constructed antenna offered only limited bandwidth and a very low peak gain. A dual-frequency printed dipole loaded with SRRs was found to offer dipolar radiation patterns with low cross-polarization. However, that antenna suffered from a narrow bandwidth [19]. A uniplanar dual-band compound loop antenna for wireless local area network/WiMAX applications was found to provide dual-band operation with a stable gain and high radiation efficiency. Yet, the antenna's impedance bandwidth was insufficient for many modern broadband applications [22]. Moreover, a multimode, wideband printed loop antenna based on degraded SRRs was demonstrated to have broadband characteristics as well as high radiation efficiency. However, the large overall antenna dimensions were found to impede device miniaturization when compared with other designs [23]. In addition, all the above-mentioned SRR antennas suffered from a common drawback, namely unstable and deteriorating radiation patterns, especially with increasing frequency.

Motivated by the difficulty of designing a cost-effective antenna with a wide bandwidth, compact size, and low profile, a compact broadband dipole antenna loaded with SRRs is proposed. The proposed antenna provides stable and uniform dipole-like radiation patterns, which maintain almost the same shape within a wide impedance bandwidth. The antenna consists of a printed dipole coupled to two identical SRRs. The antenna operates in three modes, and it exhibits broadband properties at a compact size. The design achieves a measured −10 dB impedance bandwidth of 1.32–2.46 GHz (60.31%) at a center frequency of 1.895 GHz, and its overall dimensions are 9.6 mm × 74.4 mm × 0.508 mm ($0.06\lambda \times 0.469\lambda \times 0.0032\lambda$ at 1.895 GHz).

The remainder of this paper is organized as follows. In Section II, the proposed antenna configuration is explained in detail, and the antenna's operating modes and radiation mechanism are discussed. In Section III, a comprehensive parametric study of the crucial design parameters is described. In Section IV, the results of experiments intended to verify and validate the proposed antenna design are presented, and the antenna's performance characteristics are described. Finally, in Section V, we present our conclusion.

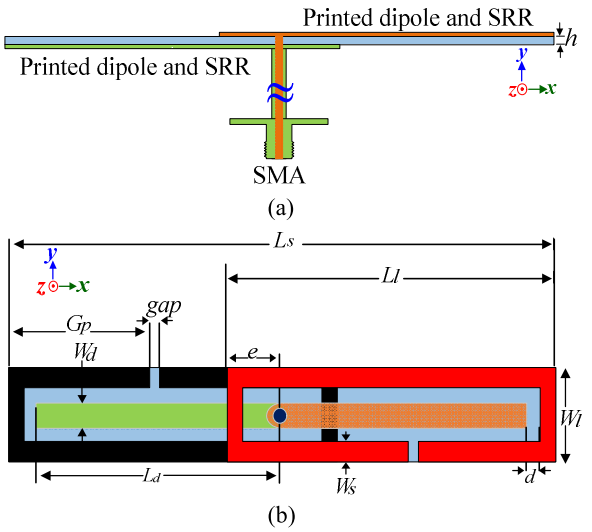

FIGURE 1. Geometry of the printed dipole loaded with SRRs: (a) side view and (b) top view.

II. ANTENNA DESIGN AND OPERATIONAL PRINCIPLES

A. ANTENNA GEOMETRY

The geometry of the proposed dipole antenna loaded with SRRs is illustrated in Fig. 1. The center-fed half-wavelength dipole is printed on the top and bottom sides of a thin dielectric substrate. The utilized substrate is a Rogers RO5880 material ($\varepsilon_r = 2.2$, $\tan\delta = 0.0009$, and $h = 0.508$ mm). Two SRRs are designed to each encircle an arm of the dipole on both sides of the substrate. The slit on each SRR is located on the opposite side with respect to the origin. The antenna is excited by a coaxial cable with a characteristic impedance of 50 Ω. The outer conductor of the coaxial line is connected to the bottom arm of the dipole, while the inner conductor of the coaxial line extends through the substrate so that it is connected to the top arm of the dipole [24]. The antenna was initially characterized computationally via

ANSYS HFSS in order to obtain a low profile, a compact size, and broadband characteristics at a center frequency of approximately 1.9 GHz. The optimized design parameters for the antenna are as follows: $e = 17.3$ mm, $W_l = 9.6$ mm, $gap = 3$ mm, $L_d = 34.7$ mm, $W_d = 3.7$ mm, $h = 0.508$ mm, $W_s = 2$ mm, $G_p = 12.2$ mm, $L_s = 74.4$ mm, and $L_l = 54.5$ mm, $d = 0.5$ mm.

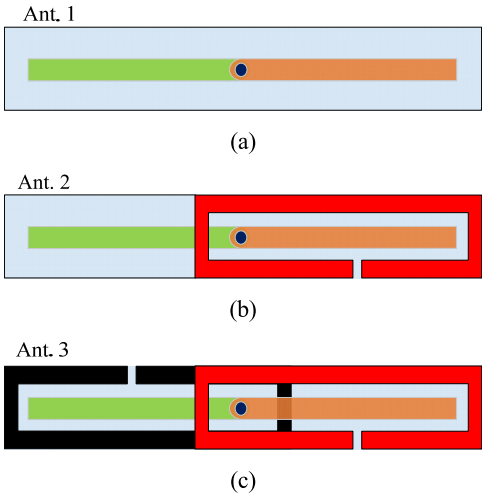

FIGURE 2. Configurations of the dipole antenna loaded with SRRs: (a) Antenna 1, (b) Antenna 2, and (c) Antenna 3.

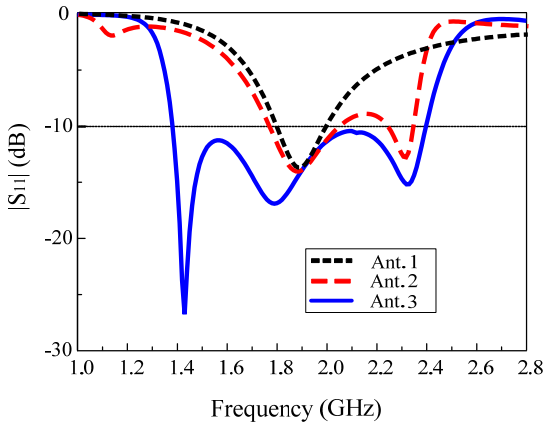

FIGURE 3. Reflection coefficient of the dipole antenna loaded with SRRs for the different antenna configurations.

B. ANTENNA OPERATING MODES AND RADIATION MECHANISM

The proposed antenna generates three resonant modes. The different modes can be understood in terms of the three configurations illustrated in Fig. 2. In Fig. 2(a), Ant. 1 contains a single radiating element, namely a conventional dipole. Ant. 2 is comprised of two elements, that is, a dipole and a single SRR on only one side of the substrate, as shown in Fig. 2(b). Ant. 3 is the proposed antenna configuration, which consists of a dipole and two SRRs, as seen in Fig. 2(c). As shown in Fig. 3, Ant. 1 produces a single mode, which originates from the single radiating half-wavelength element. Further, Ant. 2 produces two modes. The first of these modes is the dipole operating at a half-wavelength, while the additional mode results from the introduction of a single SRR, which resonates in order to produce the second mode at a higher frequency. The SRR resonates at a high frequency because its resonant length is shorter than that of the dipole. Ant. 3 is the proposed antenna structure. In this configuration, three resonant modes are generated. The intermediate-frequency resonance corresponds to the dipole mode (i.e., second mode), while the other two modes occur because both SRRs resonate in unison so as to produce resonances at both low and high frequencies. More specifically, the first mode occurs because the entire lengths of both SRRs resonate in unison as a dipole in order to produce a low-frequency resonance (1.42 GHz). This occurs at a low frequency due to the long resonant lengths provided by the SRRs. At a high frequency (2.33 GHz), the third mode results from the partial excitation of the SRRs. This partial excitation of both SRRs is noticeable as high currents within the area wherein the SRRs overlap (Fig. 3). In this mode, only the overlapping regions of both SRRs resonate at a half-wavelength. The area in which the SRRs overlap is crucial in terms of controlling the effective resonant length and, therefore, the interaction between the SRRs in this mode. The three modes interact in tandem with each other to produce a wide impedance bandwidth.

SRRs are generally composed of two metallic concentric and coupled rings with slits on opposite ends. This configuration was first proposed by Pendry *et al.* [25] in 1999 to construct a negative permeability medium. The physical mechanism of SRRs can be described as follows. When the rings are excited by an external time-varying magnetic field in the axial direction, an electromotive force is generated around the rings, which in turn generates a current in the rings [20]. SRRs are very important in relation to the design of electrically small antennas [26], [27]. One major advantage of the SRR is its ability to effectively couple to other radiating elements and produce strong resonances from strong electromagnetic interactions.

To ensure the effective operation of the SRRs, gaps (slits) are located in optimal positions on the SRRs in order to facilitate efficient coupling to the dipole and produce the desired linear polarization of the antenna. The principle behind the mechanism can be understood in terms of the surface current distribution of the proposed antenna. The surface current distributions at the resonant frequencies of 1.42, 1.8, and 2.33 GHz are studied, as shown in Fig. 4. Fig. 4(a) shows that strong currents are concentrated along the entire lengths of both SRRs at 1.42 GHz. Consequently, both SRRs are fully excited and thus radiate as the arms of a dipole with a half-wavelength resonant length. Hence, the antenna resonates at a low frequency. Furthermore, at the intermediate-frequency resonance of 1.8 GHz, a slightly weaker current distribution pattern can easily be seen on the SRRs when compared to that seen at 1.42 GHz, as shown in Fig. 4(b). The currents accumulate to a greater degree on the dipole and excite it to radiate. The dipole then resonates at a half-wavelength to produce the

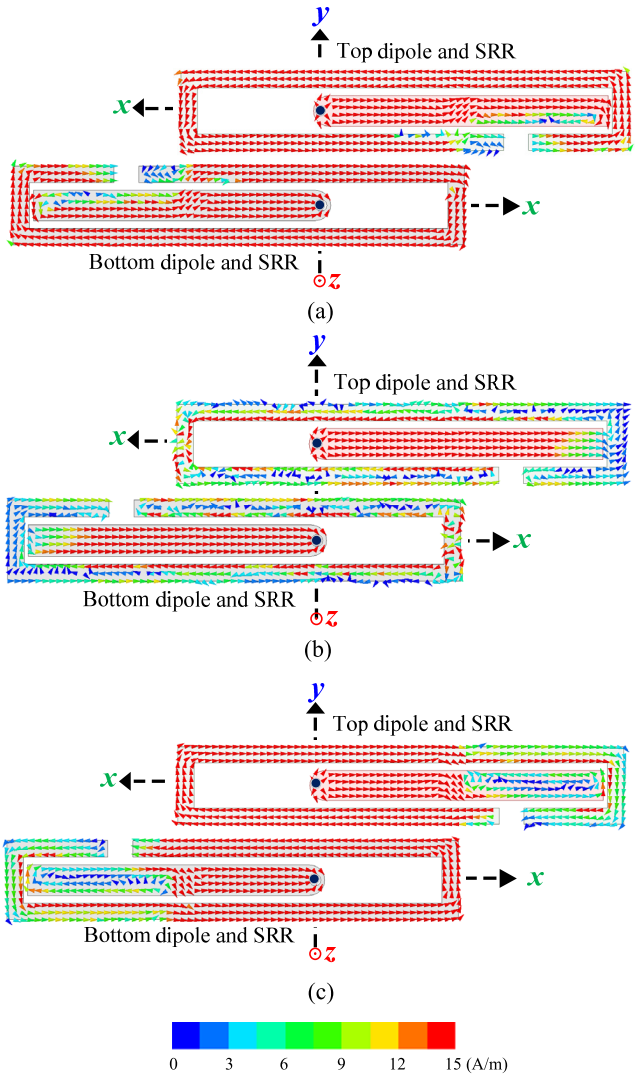

FIGURE 4. Surface current distribution on the dipole loaded with SRRs: (a) 1.42 GHz, (b) 1.8 GHz, and (c) 2.33 GHz.

intermediate-frequency resonance. At a high frequency of 2.33 GHz, the SRRs are strongly coupled to the dipole, with strong currents being seen on the overlapping regions of the two SRRs, as shown in Fig. 4(c).

Outside the overlapping regions, the current decays rapidly due to the presence of the slit, which acts as an open circuit. The strong current constantly circulates around the overlapping regions of the SRRs, thereby exciting them to radiate at a half-wavelength and generate the high-frequency mode. The position of the gap determines the length of the SRR through which the current circulates. Hence, the above-mentioned three resonances interact considerably to yield wide bandwidth characteristics. From the demonstrated symmetric current distribution on both the dipole and SRRs, the antenna produces a dipole-like omnidirectional 3-D radiation pattern with good symmetricity and nearly constant HPBWs of approximately $76° \pm 4°$ on both the xz- and xy-planes within the impedance bandwidth. The pattern retains its shape within the antenna bandwidth and it is illustrated in Fig. 5.

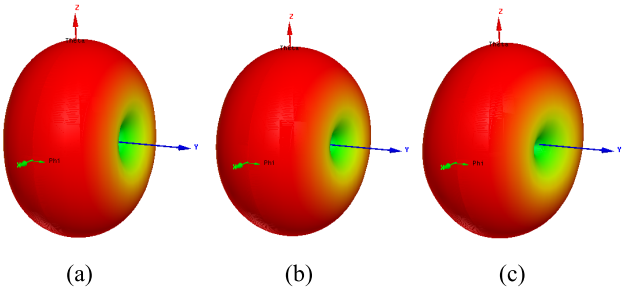

FIGURE 5. Simulated 3-D total gain pattern of the dipole loaded with SRRs: (a) 1.42 GHz, (b) 1.8 GHz, and (c) 2.33 GHz.

The antenna's resonant lengths are useful in developing approximate formulas for the estimation of the frequency of each resonance. The dipole is designed to resonate at half-wavelengths with resonant lengths equal to twice the length (L_d) of each dipole arm. Therefore, the resonant frequency of the dipole (f_d) can be deduced as

$$f_d \approx \frac{c}{2\sqrt{\varepsilon_{eff}}\,(2L_d)} \tag{1}$$

where c represents the speed of light in free space and

$$\varepsilon_{eff} \approx \frac{1+\varepsilon_r}{2} \tag{2}$$

where $\varepsilon_{\mathbf{r}}$ represents the dielectric constant of the substrate. Low-frequency resonance arises from the entire lengths of both SRRs oscillating at half-wavelengths to the dipole. The low-frequency resonance (f_L) can be estimated as

$$f_L \approx \frac{c}{2\sqrt{\varepsilon_{eff}}\,(L_s)} \tag{3}$$

High-frequency resonance arises from the overlapping area where the high currents circulate and, consequently, the resonant frequency (f_H) can be estimated as

$$f_H \approx \frac{c}{2\sqrt{\varepsilon_{eff}}\left[(L_l - G_p) - W_L\right]} \tag{4}$$

III. PARAMETRIC STUDY

The impact of the principal antenna design parameters on the antenna's performance was investigated. First, the response of the antenna was noted when all the design parameters were fixed at their optimal values. Second, during the parametric study, only one design parameter was varied at a time.

A. EFFECT OF THE DIPOLE PARAMETERS

The main parameters of the dipole are the length and the width. The effect of the dipole's length is shown in Fig. 6. A parametric study of the dipole's length clearly shows that the dipole is responsible for the intermediate-frequency resonance. When the dipole's length is increased or decreased, the SRRs' lengths remain the same, as do the overlapping regions of the two SRRs. A decrease in the dipole's resonant length causes a shift to the right in the antenna impedance curve, whereas the other two resonant points remain unaffected, meaning that they do not move from their

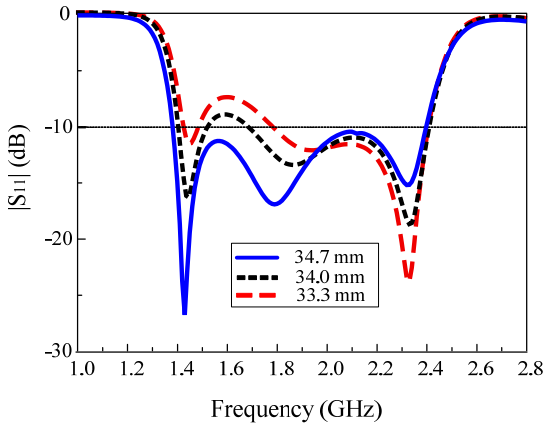

FIGURE 6. Reflection coefficient of the dipole antenna loaded with SRRs for various dipole lengths (L_d).

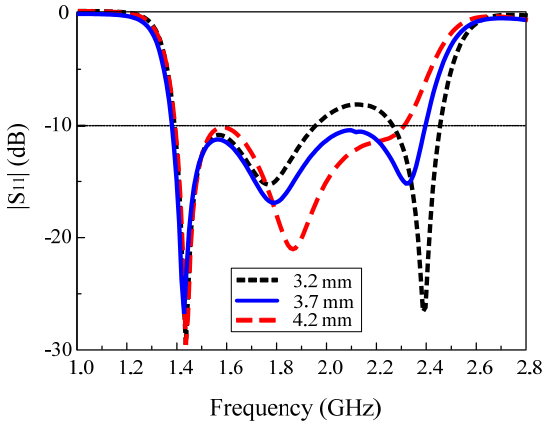

FIGURE 7. Reflection coefficient of the dipole antenna loaded with SRRs for various dipole widths (W_d).

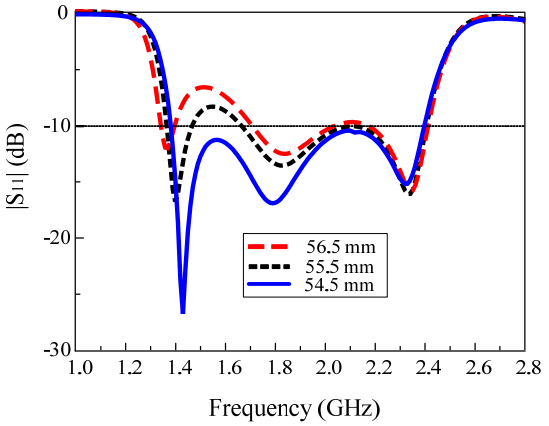

FIGURE 8. Reflection coefficient of the dipole antenna loaded with SRRs for various SRR lengths (L_l).

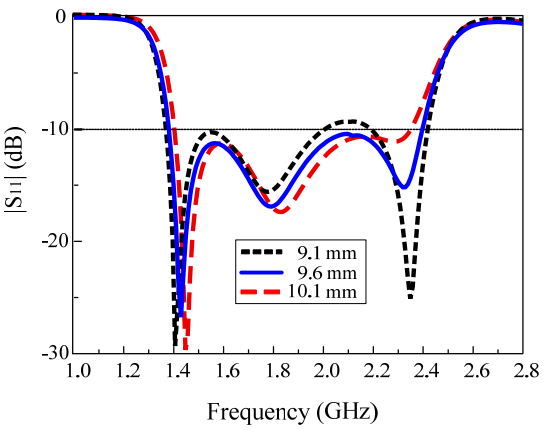

FIGURE 9. Reflection coefficient of the dipole antenna loaded with SRRs for various SRR widths (W_l).

resonant frequencies. The movement of the intermediate-frequency resonance that occurs following a change in the dipole's length confirms that the dipole generates this mode. At 34.7 mm, the dipole provides the optimal resonant length for the other two resonances to interact and, consequently, generate a broad bandwidth.

When the dipole's width is varied from 3.2 to 4.2 mm, the coupling between the dipole and the SRRs varies. As the width increases, the coupling decreases. In the case of a small dipole width, the dipole becomes over coupled to the SRRs, whereas in the case of a large dipole width, it becomes under coupled. Accordingly, there is an optimal dipole-SRR separation point at which critical coupling occurs between the two elements. Therefore, the dipole's width is significant in terms of controlling the coupling between the dipole and the SRRs. This response has a greater impact at high frequencies than at low frequencies. Thus, the dipole's width is essential in relation to impedance matching at high frequencies, as demonstrated in Fig. 7.

B. EFFECT OF THE SRR PARAMETERS

The SRR has three major parameters. First, the length of the SRR is significant in terms of determining the antenna's operational frequencies, as shown in Fig. 8. The length of the SRR was increased horizontally away from the center of the antenna with no change in the overlapping regions of the SRRs. As the resonant length increased, a predictable response was observed, namely a shift in the lowest resonance point to lower frequencies. Only the low-frequency mode moved. Indeed, the other two high-resonance points maintained their positions, thereby providing further evidence that both SRRs are responsible for the lowest-frequency resonance. Second, Fig. 9 shows the effects of the SRR's width (W_l). This parameter controls the level of interaction between the dipole and the SRRs. As the W_l increases, the coupling decreases. The dipole's width and the SRR's width have similar effects on the interaction (or coupling) between the dipole and the SRRs. Fig. 10 shows the effect of the SRR's stripline width, which affects the coupling at both low and high frequencies. These two resonance points are generated by the SRRs. Moreover, at an SRR stripline width of 2 mm, both the high and low frequencies are well matched. This parameter is essential in terms of matching both the lower and higher frequencies of the antenna.

The area of overlap between the two SRRs, as represented by $2e$, significantly affects the antenna's radiation modes.

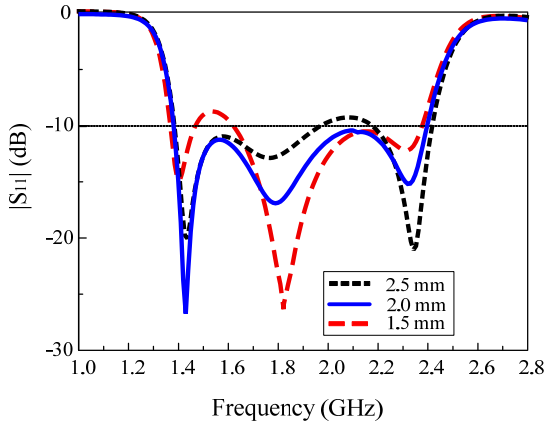

FIGURE 10. Reflection coefficient of the dipole antenna loaded with SRRs for various SRR stripline widths he (W_s).

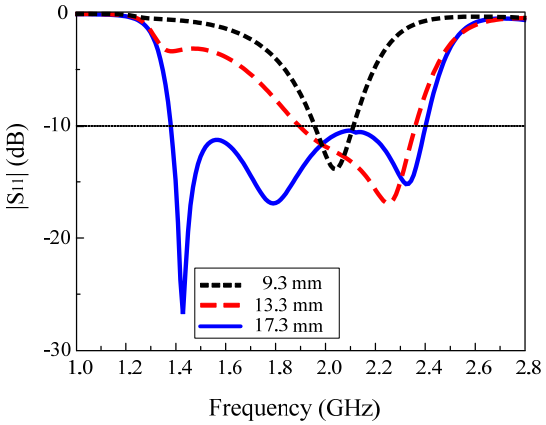

FIGURE 11. Reflection coefficient of the dipole antenna loaded with SRRs for various overlap lengths between the SRRs (2e).

Fig. 11 shows the response of the antenna when the overlapping region of the SRRs is varied. The response to variations in this area of overlap provides further evidence of the simultaneous operation of both SRRs in order to generate the first and third modes. At an overlap length of less than 9 mm, the antenna only operates in the dipole mode, thereby generating a single resonance. The dipole and the SRRs are not effectively coupled to each other. Yet, as the overlap length increases, the coupling between the dipole element and the SRRs increases. At an overlap length of greater than 10 mm, the coupling becomes strong enough to excite both SRRs so as to generate two additional resonances.

Moreover, at the optimal overlap distance of 17.3 mm, the interaction between the SRRs reaches its maximum level, and both SRRs become strongly coupled to the dipole. The SRRs operate in unison as the arms of the dipole in order to produce the low- and high-frequency modes.

The position of the SRR gap is one of the most critical design parameters, because it not only significantly affects the impedance matching, but also influences the cross-polarization level of the antenna. The antenna responds differently depending on the position of the gap. When the gap on the SRR is close to the center of the antenna ($G_p = 34.2$ mm, Fig. 12), the antenna does not resonate within the desired

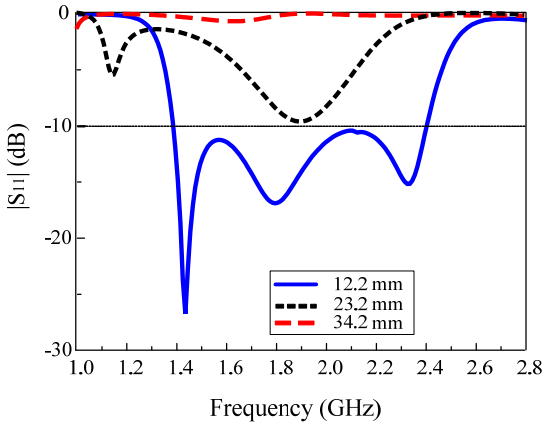

FIGURE 12. Reflection coefficient of the dipole antenna loaded with SRRs for various SRR gap positions (G_p).

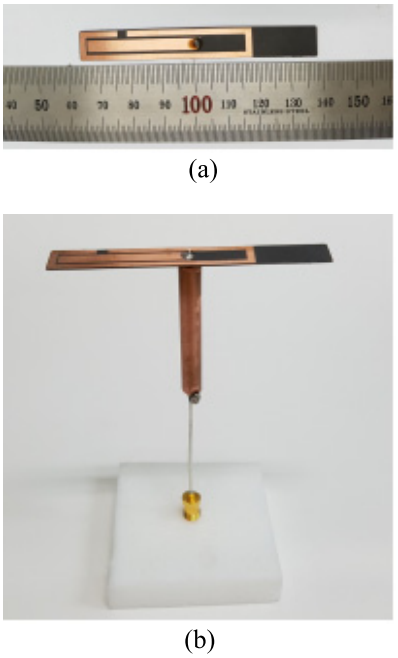

FIGURE 13. Fabricated sample of the proposed antenna with a balun: (a) top view and (b) three-dimensional view.

frequency ranges, which results in poor impedance matching. This configuration produces very high cross-polarization. Furthermore, as the position of the gap (G_p) moves away from the center of the antenna toward a point halfway along the SRR ($G_p = 23.2$ mm, Fig. 12), the antenna responds differently. This configuration generates two resonances with high cross-polarization. When the G_p is located far from the center of the antenna ($G_p = 12.2$ mm, Fig. 12), the optimal antenna characteristics are obtained. The cross-polarization becomes very small, while symmetrical radiation patterns are produced with broadband impedance matching. Hence, the positioning of the gap can be used to minimize cross-polarization while matching the antenna.

IV. EXPERIMENTAL RESULTS

A rigid 50-Ω coaxial cable with balun is used to feed the fabricated antenna, as shown in Fig. 13. The balun is designed

to operate at a quarter-wavelength. The inner conductor of the coaxial cable is soldered to the top arm of the dipole, and the outer conductor of the coaxial cable is soldered to the bottom arm of the dipole. The balun extends along the coaxial cable; it is soldered to the outer conductor at the bottom of the balun to eliminate the common mode current flowing on the outer conductor of the coaxial cable, and to avoid radiation pattern distortion, especially at high frequencies. The antenna has overall dimensions of 9.6 mm × 74.4 mm × 0.508 mm ($0.06\lambda \times 0.469\lambda \times 0.0032\lambda$ at 1.895 GHz) as well as a broad impedance bandwidth. The prototype's reflection coefficient was measured using an Agilent N5230A network analyzer and a 3.5 mm coaxial calibration standard (GCS35M). The far-field measurements were made in a full anechoic chamber with the dimensions of 15.2 m (W) × 7.9 m (L) × 7.9 m (H) at the RFID/USN Center, Incheon, Korea. During the radiation pattern measurement procedure, a standard wideband horn antenna was used for transmitting, while the proposed antenna was used for receiving. The transmitter and the receiver were separated by a distance of 10 m. The horn antenna was fixed, while the proposed dipole antenna loaded with SRRs was rotated from −180° to 180° at a scan angle of 1° and a speed of 3° s^{-1}.

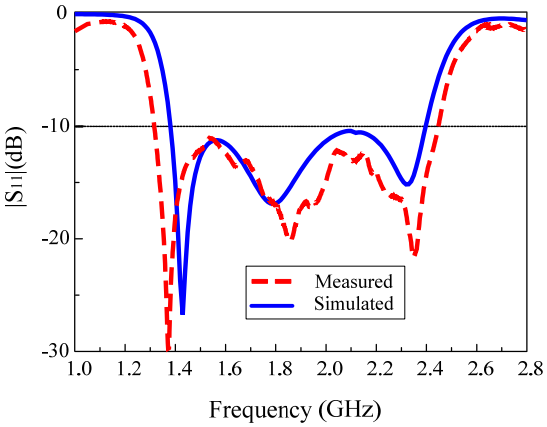

FIGURE 14. Measured and simulated reflection coefficient values.

Fig. 14 shows the measured and simulated reflection coefficients of the fabricated antenna. Minute disparities were observed between the measurements and the HFSS simulation which could be associated with misalignment or with inconsistencies during the antenna fabrication process. However, both results establish that the prototype exhibited wideband operation. As shown in Fig. 14, the measured impedance bandwidth at a reflection coefficient of less than −10 dB is 1.32–2.46 GHz (60.31%), while the simulated bandwidth is 1.38–2.41 GHz (54.35%).

The radiation patterns and broadside gain of the fabricated prototype at different frequencies were measured, and they are shown in Figs. 15 and 16, respectively. The antenna generates good broadside dipole-like radiation patterns, with a symmetrical profile and negligible fluctuations in gain within the entire impedance bandwidth. The radiation patterns are almost constant and show little or no deterioration

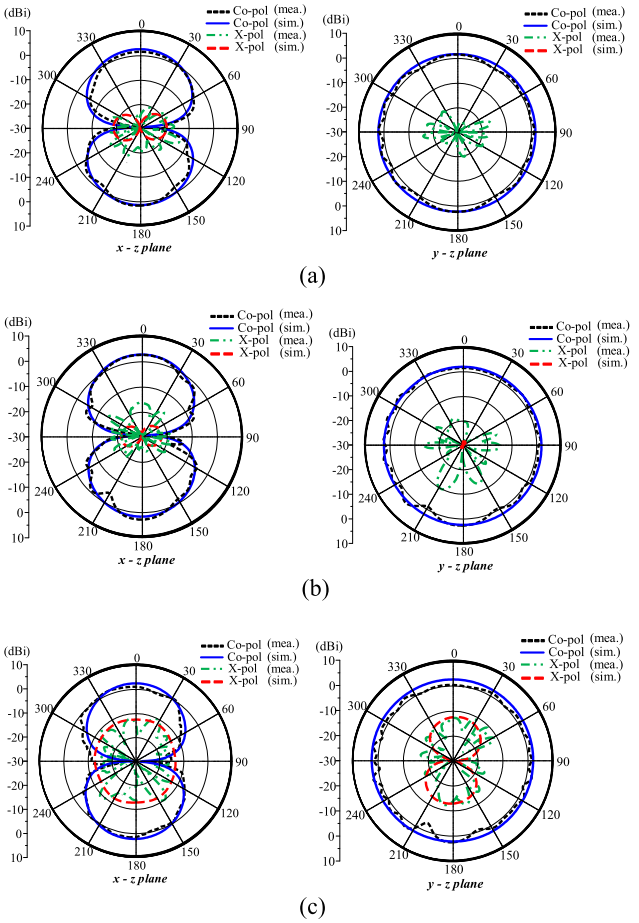

FIGURE 15. Measured and simulated radiation patterns of the dipole antenna loaded with SRRs: (a) 1.42 GHz, (b) 1.8 GHz, and (c) 2.33 GHz.

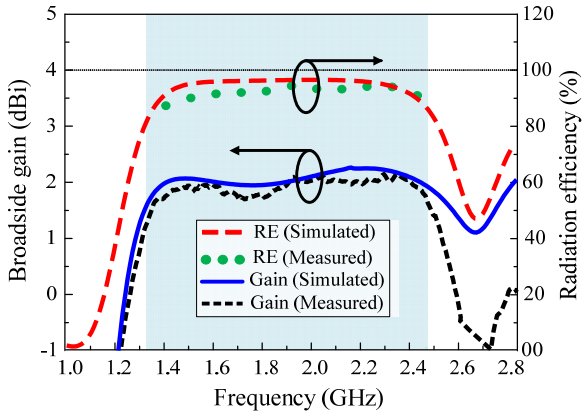

FIGURE 16. Measured and simulated broadside gain of the dipole antenna loaded with SRRs.

with increasing frequency. The cross-polarization is 14 dB less than the co-polarization in both the x–z and y–z planes within the impedance bandwidth of the antenna. The radiation patterns are fairly symmetrical in both the x–z and y–z planes. The measurement results indicate some ripples in the radiation patterns. These ripples are attributed to the effects of the foam rack and tapes employed in the pattern measurement setup.

TABLE 1. Performance comparison of the proposed antenna with other antenna designs.

Antenna structure	Size (λ^3)[a]	−10 dB $\lvert S_{11}\rvert$ BW (%, GHz)	Rad. type[b]	Peak gain (dBi)	Radiation efficiency (%)
Ref. [1]	0.363 × 0.363 × 0.0024	49 0.7–1.15	Uni	4.8	-
Ref. [14]	0.548 × 0.6478 × 0.0986	10.8 1.414–1.576	Bi	0.7	65
Ref. [16]	0.31 × 0.63 × 0.0063	44.2 1.85-2.9	Bi	4.7	-
Ref. [17]	0.129 × 0.129 × 0.0106	7.21 1.923–2.073	Bi	−4.8	-
Ref. [18][c]	0.081 × 0.081 × 0.005	3.61, 5.55 0.917–0.950, 1.506–1.593	Bi	-	36.7 43.6
Ref. [23]	0.575 × 0.575 × 0.0115	67 2.3–4.6	Uni	5.1	80
Proposed	0.06 × 0.469 × 0.0032	60.31 1.32–2.46	Bi	2.1	88

[a]λ is the free-space wavelength with respect to the center frequency of the impedance bandwidth. [b]Uni: unidirectional, bi: bidirectional. [c]Dual-band antenna.

At 1.42 GHz, the measurements showed a half-power beamwidth (HPBW) of 64.26° in the y–z plane and a broadside gain of 1.9 dBi. At 1.8 GHz, the prototype yielded a measured HPBW of 66.38° in the y–z plane and a broadside gain of 1.85 dBi. Further, at 2.33 GHz, the measurements indicated a HPBW of 54.48° in the y–z plane and a broadside gain of 2.0 dBi. Fig. 16 compares the simulated and measured broadside gains of the fabricated antenna. The antenna gain increased steadily, before reaching a maximum value of 2.1 dBi at 2.14 GHz. The measurements indicated a peak gain of 2.1 dBi and high radiation efficiency of $> 88\%$ across the operational bandwidth. Table I compares the performance of the proposed antenna to that of other antenna designs featuring SRRs described in the literature.

V. CONCLUSION

A broadband, compact, low-profile dipole antenna loaded with two SRRs is presented in this paper. Each radiating element makes a noticeable contribution to the generation of three resonances. As a result, the proposed antenna exhibits broadband characteristics. A distinguishing feature of the proposed antenna is its compactness and low profile when compared with similar designs featuring SRRs. The antenna also offers stable, symmetrical, and non-deteriorating omnidirectional radiation patterns, which give it an advantage over its counterparts. The experimental and simulated results demonstrate good performance characteristics, namely a wide bandwidth, stable gain, symmetric radiation patterns, and high radiation efficiency.

These properties, when combined with its low profile, light weight, and compact size, render the proposed antenna a potential candidate for use in many modern wireless communication systems, especially for the Internet of Things and in wearable applications. The proposed antenna provides broadband qualities, and further bandwidth enhancement through other techniques provides opportunities for additional research. Another potential research avenue is increasing antenna flexibility by employing 3-D printing techniques to make the antenna an even more suitable candidate for the Internet of Things and in wearable applications.

REFERENCES

[1] S. A. Rezaeieh and A. M. Abbosh, "Compact planar loop-dipole composite antenna with director for bandwidth enhancement and back radiation suppression," *IEEE Trans. Antennas Propag.*, vol. 64, no. 8, pp. 3723–3728, Aug. 2016.

[2] K. Ding, C. Gao, D. Qu, and Q. Yin, "Compact broadband MIMO antenna with parasitic strip," *IEEE Antennas Wireless Propag. Lett.*, vol. 16, pp. 2349–2353, 2017.

[3] H. W. Lai and H. Wong, "Substrate integrated magneto-electric dipole antenna for 5G Wi-Fi," *IEEE Trans. Antennas Propag.*, vol. 63, no. 2, pp. 870–874, Feb. 2015.

[4] K. Ding, C. Gao, B. Zhang, Y. Wu, and D. Qu, "A compact printed unidirectional broadband antenna with parasitic patch," *IEEE Antennas Wireless Propag. Lett.*, vol. 16, pp. 2341–2344, 2017.

[5] J. Wu, Z. Zhao, Z. Nie, and Q. H. Liu, "A broadband unidirectional antenna based on closely spaced loading method," *IEEE Trans. Antennas Propag.*, vol. 61, no. 1, pp. 109–116, Jan. 2013.

[6] M. Kong, G. Shin, S.-H. Lee, and I.-J. Yoon, "Investigation of 3D printed electrically small folded spherical meander wire antenna," *J. Electromagn. Eng. Sci.*, vol. 17, no. 4, pp. 228–232, Oct. 2017.

[7] S.-W. Qu, J.-L. Li, Q. Xue, and C.-H. Chan, "Wideband periodic endfire antenna with bowtie dipoles," *IEEE Antennas Wireless Propag. Lett.*, vol. 7, pp. 314–317, 2008.

[8] C. F. Tseng and C. L. Huang, "A wideband cross monopole antenna," *IEEE Trans. Antennas Propag.*, vol. 57, no. 8, pp. 2464–2468, Aug. 2009.

[9] T.-G. Ma and S.-K. Jeng, "A printed dipole antenna with tapered slot feed for ultrawide-band applications," *IEEE Trans. Antennas Propag.*, vol. 53, no. 11, pp. 3833–3836, Nov. 2005.

[10] N.-W. Liu, L. Zhu, W.-W. Choi, and X. Zhang, "A low-profile aperture-coupled microstrip antenna with enhanced bandwidth under dual resonance," *IEEE Trans. Antennas Propag.*, vol. 65, no. 3, pp. 1055–1062, Mar. 2017.

[11] N.-W. Liu, L. Zhu, W.-W. Choi, and X. Zhang, "Wideband shorted patch antenna under radiation of dual-resonant modes," *IEEE Trans. Antennas Propag.*, vol. 65, no. 6, pp. 2789–2796, Jun. 2017.

[12] J. Wu, Z. Zhao, Z. Nie, and Q. H. Liu, "A printed unidirectional antenna with improved upper band-edge selectivity using a parasitic loop," *IEEE Trans. Antennas Propag.*, vol. 63, no. 4, pp. 1832–1837, Apr. 2015.

[13] S. A. Rezaeieh, A. Zamani, K. S. Bialkowski, and A. M. Abbosh, "Unidirectional slot-loaded loop antenna with wideband performance and compact size for congestive heart failure detection," *IEEE Trans. Antennas Propag.*, vol. 63, no. 10, pp. 4557–4562, Oct. 2015.

[14] W.-T. Hsieh and J.-F. Kiang, "Small broadband antenna composed of dual-meander folded loop and disk-loaded monopole," *IEEE Trans. Antennas Propag.*, vol. 59, no. 5, pp. 1716–1720, May 2011.

[15] W.-J. Lu, G.-M. Liu, K. F. Tong, and H.-B. Zhu, "Dual-band loop-dipole composite unidirectional antenna for broadband wireless communications," *IEEE Trans. Antennas Propag.*, vol. 62, no. 5, pp. 2860–2866, May 2014.

[16] D.-L. Wen, Y. Hao, H.-Y. Wang, and H. Zhou, "Design of a wideband antenna with stable omnidirectional radiation pattern using the theory of characteristic modes," *IEEE Trans. Antennas Propag.*, vol. 65, no. 5, pp. 2671–2676, May 2017.

[17] P. Chen, L. Peng, A. Wu, and G. Wang, "Rendering wide impedance band of ESA made of SRRs," *Electron. Lett.*, vol. 52, no. 19, pp. 1582–1584, Sep. 2016.

[18] L. Wang, M. Q. Yuan, and Q. H. Liu, "A dual-band printed electrically small antenna covered by two capacitive split-ring resonators," *IEEE Antennas Wireless Propag. Lett.*, vol. 10, pp. 824–826, 2011.

[19] F. J. Herraiz-Martínez, L. E. García-Muñoz, D. Gonzalez-Ovejero, V. González-Posadas, and D. Segovia-Vargas, "Dual-frequency printed dipole loaded with split ring resonators," *IEEE Antennas Wireless Propag. Lett.*, vol. 8, pp. 137–140, 2009.
[20] M.-C. Tang and R. W. Ziolkowski, "A study of low-profile, broadside radiation, efficient, electrically small antennas based on complementary split ring resonators," *IEEE Trans. Antennas Propag.*, vol. 61, no. 9, pp. 4419–4430, Sep. 2013.
[21] M. Li, X. Q. Lin, J. Y. Chin, R. Liu, and T. J. Cui, "A novel miniaturized printed planar antenna using split-ring resonator," *IEEE Antennas Wireless Propag. Lett.*, vol. 7, pp. 629–631, 2008.
[22] F. Liu, K. Xu, P. Zhao, L. Dong, and G. Wang, "Uniplanar dual-band printed compound loop antenna for WLAN/WiMAX applications," *Electron. Lett.*, vol. 53, no. 16, pp. 1083–1084, Jun. 2017.
[23] K. Xu, F. Liu, L. Peng, W.-S. Zhao, L. Ran, and G. Wang, "Multimode and wideband printed loop antenna based on degraded split-ring resonators," *IEEE Access*, vol. 5, pp. 15942–15947, 2017.
[24] S. X. Ta, I. Park, and R. W. Ziolkowski, "Broadband electrically small circularly polarized directive antenna," *IEEE Access*, vol. 5, pp. 14657–14663, 2017.
[25] J. B. Pendry, A. J. Holden, D. J. Robbins, and W. J. Stewart, "Magnetism from conductors and enhanced nonlinear phenomena," *IEEE Trans. Microw. Theory Techn.*, vol. 47, no. 11, pp. 2075–2084, Nov. 1999.
[26] R. W. Ziolkowski and A. Erentok, "Metamaterial-based efficient electrically small antennas," *IEEE Trans. Antennas Propag.*, vol. 54, no. 7, pp. 2113–2130, Jul. 2006.
[27] A. Erentok and R. W. Ziolkowski, "Metamaterial-inspired efficient electrically small antennas," *IEEE Trans. Antennas Propag.*, vol. 56, no. 3, pp. 691–707, Mar. 2008.

KAM EUCHARIST KEDZE received the B.Tech. degree in electrical and electronic engineering (tele-communication) from the University of Buea, Cameroon, in 2013. He is currently pursuing the M.S./Ph.D. degree with the Department of Electrical and Computer Engineering, Ajou University, Suwon, South Korea. His research interests include design of patch antennas, crossed-dipole antennas, miniaturized antennas, and metasurface antennas.

HEESU WANG received the B.Sc. degree in electrical and computer engineering from Ajou University, Suwon, South Korea, in 2018, where he is currently pursuing the M.S. degree with the Department of Electrical and Computer Engineering. His research interests include design of patch antenna, printed antennas, small antennas, and metasurface antennas for various wireless applications.

IKMO PARK received the B.S. degree in electrical engineering from The State University of New York at Stony Brook, and the M.S. and Ph.D. degrees in electrical engineering from the University of Illinois at Urbana–Champaign. He has been with the Device & Materials Laboratory, LG Corporate Institute of Technology, Seoul, South Korea, where he has been involved in research and development of various antennas for personal communication systems, wireless local area networks, and direct broadcasting systems. He joined the Department of Electrical and Computer Engineering, Ajou University, in 1996. He was a Visiting Professor with the Department of Electrical and Computer Engineering, POSTECH, Pohang, South Korea, from 2004 to 2005, and also with the Department of Electrical and Computer Engineering, University of Arizona, Tucson, AZ, USA, from 2011 to 2012.

He has authored and co-authored over 300 technical journal and conference papers. He holds over 40 domestic and international patents. He is also a member of Eta Kappa Nu and Tau Betta Pi. He is a member of the Board of Directors at the Korea Institute of Electromagnetic Engineering and Science (KIEES). He has served as the Chair of the Department of Electrical and Computer Engineering, Ajou University. He serves as the Editor-in-Chief for the *Proceeding of the KIEES* and *Journal of KIEES*, an Editorial Board member for the *International Journal of Antennas and Propagation*, and an Associate Editor of the *IET Electronics Letters*. He has served as an Editorial Board member for the *Journal of Electromagnetic Engineering and Science*.

His current research interests include the design and analysis of microwave, millimeter-wave, terahertz wave, and nano-structured antennas. He serves as the chair, organizer, and a member of the program committees for various conferences, workshops, and short courses in electromagnetic related topics. He is also a frequent reviewer for over 10 scientific journals and book publishers.

He was a recipient of several awards and recognitions, including the KIEES Outstanding Scholarly Achievement Award in 2014, the KIEES Outstanding Researcher Award in 2013, the KIEES Distinguished Service Award in 2012, the KIEES Meritorious Award in 2015, the Ajou Publication Award in 2013, the Ajou Dasan Research Award in 2017 and 2018, respectively, the Distinguished Service Award from the Department of Electrical and Computer Engineering, Ajou University, in 2011, the Outstanding Advisor Award from Radio Engineering and Research Center, KAIST, in 2009, the Best Paper Award from Optical Society of Korea in 2007, the Best Paper Award from KIEES in 2010 and 2016, respectively, the IEEE iWAT Best Poster Paper Award in 2005, and the Haedong Best Paper Award from the Institute of Electronics Engineers of Korea in 2002.